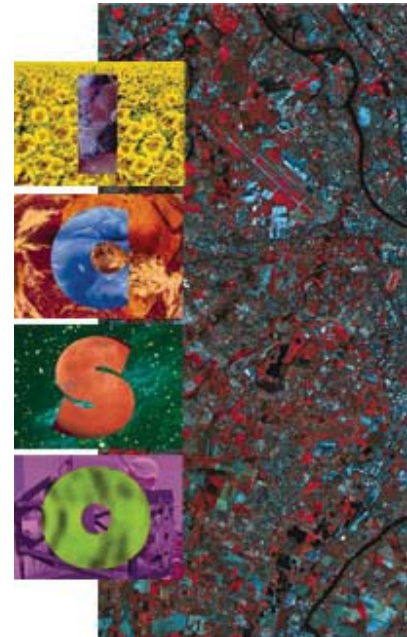


# International Conference on Space Optics—ICSO 2000

Toulouse Labège, France

5–7 December 2000

*Edited by George Otrio*



## *Stray light in Picard telescope*

*Pierre Etcheto, Anne Macaire*



ics0 proceedings



## Stray light in PICARD Telescope

Pierre ETCHETO, Anne MACAIRE

*CNES, DTS/AE/INS/TO*

**Résumé :** L'instrument spatial PICARD observe le Soleil dans le lointain UV et le visible. Il requiert une très grande précision géométrique et radiométrique pour mesurer le diamètre local du Soleil. Cet instrument est donc très sensible à la lumière parasite. Les réflexions multiples entre le détecteur, les miroirs et les filtres ont été modélisées avec ASAP 6. Elles ne sont pas très critiques pour une source ponctuelle, mais pour une source large elles ajoutent un signal important, qui fausse le profil du bord du Soleil. La diffusion des optiques près du spéculaire étale aussi la tache image, surtout pour les courtes longueurs d'onde. La diffusion des baffles et structures est moins critique, mais leur conception doit être soignée. Pour remplir la mission, cette lumière parasite doit être estimée très précisément à partir de mesures, puis prise en compte dans le traitement d'image. La précision dépend de l'échantillonnage du modèle, des caractéristiques et de la pollution des optiques, et de l'orientation des roues à filtres.

**Abstract:** *The PICARD space borne instrument observes the Sun from far UV to visible wavelengths. Very high geometrical and radiometric accuracy is required to measure the Sun's local diameter. Thus this instrument is very sensitive to stray light. Multiple reflections between the detector, the mirrors and the filters have been modelled with ASAP 6. They are not very critical for a point source, but for a broad source they add a notable contribution, biasing the edge of the Sun image. Near specular scatter from optics also enlarges the instrumental response, especially at short wavelengths. Scatter from baffles and structures is less critical, but the later need a careful design. To fulfil the mission, stray light shall be predicted very accurately, based on measured data, then taken into account in the image processing. Accuracy depends on the model sampling, the reflectivity and contamination of optics, and the misalignments of the filter wheels.*

### 1- INTRODUCTION

PICARD is being developed by the Service d'Aéronomie, a French CNRS laboratory [Dam98], [Dam00]. One of its missions is to measure the Sun local diameter with an accuracy of  $10^{-3}$  arcsec. The Sun edge slope spreads over about 7 pixels. Its middle is calculated, then averaged over the Sun contour. Other missions include imaging the Sunspots with a lesser resolution. The focal length shall be periodically calibrated on stars.

To comfort the instrument preliminary design, stray light has been studied at 230 nm. Its geometrical behaviour and order of magnitude was estimated, and its effect on instrumental performances discussed. The ASAP model includes optical components, baffles and visible structures, after the preliminary definition. Optical surfaces features are based on manufacturers data, measured samples and typical values.

## 2- INSTRUMENT MODEL

### 2-1- TELESCOPE

The SODISM telescope is a Ritchey - Chrétien with two filter wheels and a back-illuminated CCD detector. Its geometrical features are:

- Focal length : 2650 mm
- Aperture : 110 mm, minus central obscuration.
- Field of view: 36 x 36 arcmin (Sun : 32 arcmin)
- Resolution: Pixel FOV = 1 arcsec. PSF  $\simeq$  0,5 arcsec. Best focus at field edge.
- Spectral bands: 121.6 nm, 160 nm, 230 nm, 548 nm. Bandwidth 8 nm.

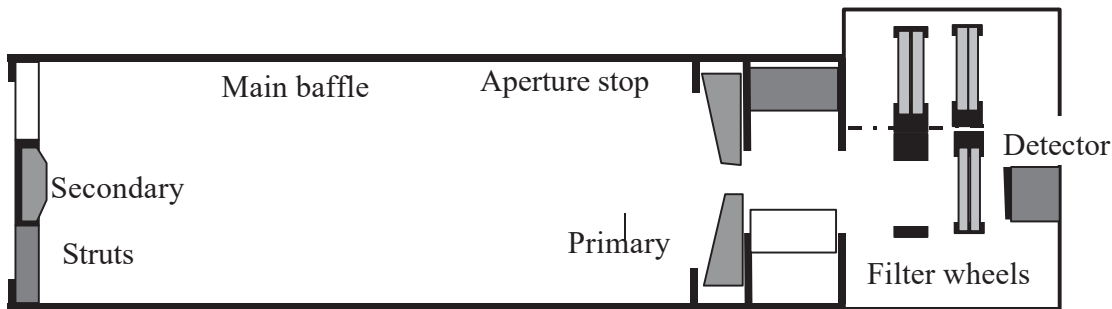


**Fig. 1: PICARD instrument layout**

The mirrors are uncoated SiC-CVD, to reduce the signal and resist UV radiations. Their reflectivity has been measured by the LOSCM (Laboratoire d'Optique des Surfaces et Couches Minces, at Marseilles) : at 230 nm it is 32%. They absorb the rest. Their specified roughness is 1 nm. Scatter shall be discussed in (Ch. 3-4). Mirror edges are sanded and uncoated.

### 2-2- DETECTOR

The detector is an EEV (Marconi) 4280 back illuminated CCD matrix. The sensitive area is 27.6 mm wide, with 1024 x 1024 pixels 13.5  $\mu$ m (1 arcsec.) wide. The front surface is very smooth and the pixel structure is not seen, so that its scatter and diffraction should be negligible. But this surface is partially reflective, which causes ghost images.

If the Silicium is uncoated, its reflectivity at 230 nm, measured by the LOSCM, is 64%. But nominally the detector should bear an EEV antireflection coating, designed for the visible. Its UV reflectivity is not known, but its effect on quantum efficiency has been measured. At 230 nm, this efficiency is 10% without a coating and 20% with it. Assuming that absorption by the coating is negligible, and since the efficiency of Silicium is unchanged, only the interface transmission should vary. This transmission is 36% for uncoated Si, doubled at 72% with the coating. Therefore, the reflectivity with this coating should be 28% at most. The endurance of this coating to UV radiations is not yet secured, so both cases were studied.

### 2-3- FILTERS

The need is an 8-nm bandpass, a few percent transmission and a  $10^{-8}$  rejection. This shall be done with two specific ACTON filters, based on the manufacturer's standard 10 nm filters [Act00]. Their transmission is usually  $T = 12$  to 15%, with a  $10^{-4}$  rejection. Their reflectivity has not been measured. ACTON's latest estimate is  $R = 20$  to 30%. The rest is absorbed in the metal-dielectric layers. Nominally, the other face should be uncoated, with 4.3% reflectivity. If needed, it could have a narrow band antireflective coating, reflecting less than 0.3%. Both cases were modelled. Scatter on this face should be far lower than on the filter.

To meet the requirements, two filters are stacked face to face. They are mounted in a wheel, with an unknown air spacing. As the Sun is a (relatively) broad and incoherent source, we assume that interference between the 2 filters have no effect on the image. To simplify the model, we simulate both filter coatings with an equivalent glass - glass interface (fig.2):

$$R_{\text{éq}} = R[1+T^2/(1-R^2)] \quad (1)$$

$$T_{\text{éq}} = T^2/(1-R^2) \quad (2)$$

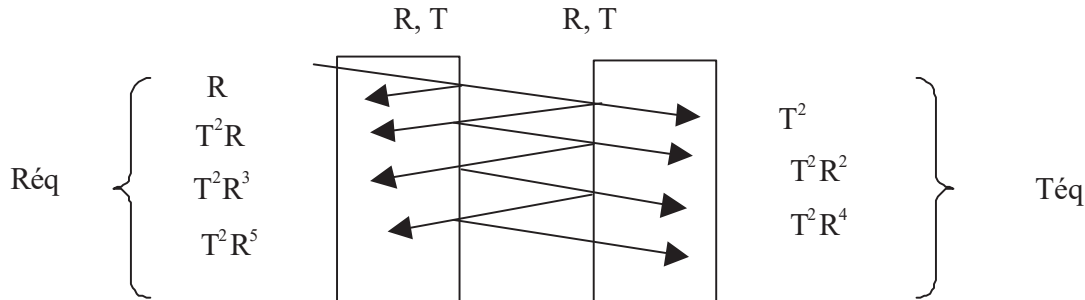


**Fig. 2: Combined reflections in the filters**

Assuming that  $T=15\%$  and  $R=20\%$ , this gives  $R_{\text{éq}}=20.47\%$  and  $T_{\text{éq}}=2.34\%$ . Before ACTON's estimates were available, other reflectivities from 10 to 85% were also modelled. To aim at stars, a broadband visible window is used. Its antireflective coating would reflect typically 1%. This configuration, less critical than the UV, was not studied.

Two filter wheels are used alternatively. The filters position along axis effects on the ghosts focusing, so both positions were modelled. The centring of both image and ghosts is very sensitive to the filters tilt. This is discussed in (Ch. 3-3-4-2).

## 2-4-BAFFLES AND STRUCTURES

These were modelled with a simplified geometry, mostly to check which areas were critical. Baffles and stops should have a black paint or anodisation. These are well known, thanks to many measurements with the CNES angle resolved scatter facility. For the ghost image analysis, mechanical elements were modelled as fully absorbing. The modelled components are the aperture stop, the screen behind the primary mirror, the stops in the wheel before and after the filters, the Peltier components (cylinders of unknown aspect), the main baffle (body and entrance vane) and the secondary mirror mount, with its sunshield and struts, as designed (cf. Ch. 4-3).

## 2-5- SOURCES

To perform stray light analysis, several sources were modelled:

- **Point source:** To check the image quality, vigneting, the build-up of ghost images and the effect of tilts. To model a star, rays shall be associated with gaussian beamlets [BRO99]. The aperture grid covers the baffle entrance with 50 x 50 rays.
- **Ideal Sun:** It is an incoherent emitting disk, covering the baffle entrance and a 32-arcmin cone with an uniform radiance and sharp edges. 100 000 rays are enough to check paths and illuminated objects, but 1 million are needed for accurate ghosts modelling at high resolution. Due to high order splits, computations take up to 6 hours with a Pentium III.
- **Real Sun:** Same source, with an apodisation simulating the edge fallout on about 7 arcsec. This is to check the contribution of the Sun edge itself on stray light in this area.
- **Detector:** An emitting surface equivalent to the detector, emitting towards the filters. This is to check critical objects.

## 3- STRAY LIGHT ANALYSIS

### 3-1- OVERVIEW

Stray light is a complex matter, involving several physical phenomena and complicated geometries. Analysis and modelling must be processed step by step, with non-sequential ray tracing by a dedicated software. We used ASAP 6.6 of BRO [BRO99]. The main steps are:

- **Model the instrument**, with realistic geometry and features (Ch. 2). Some features (ray splitting, scatter) may be omitted on some objects to study specific paths.
- **Check critical paths** first with a point source, then with a broad one. Identify critical objects which are both seen and illuminated through direct or reflected paths.
- **Model accurately** each critical path with many rays and a fine sampling, to estimate the stray signal level and profile. For this we needed 1 million rays, 8 split-levels and a 3 arcsec. sampling. This is 3 instrument pixels, but was the best possible here. As the system is axis centred, we can reduce the sampling noise with a radial average the image.
- **Check the influence** of various parameters (coatings, filter position, misalignments)...
- **Discuss the effect** on instrumental performance and possible remedies.

In PICARD, expected stray light problems were multiple reflections between the detector, the filters and the mirrors; in-field scatter by optics, and out of field scatter by mechanical components.

### 3-2- CHECKING AND IDENTIFICATION

#### 3-2-1- Image quality

The image of a point source through the nominal path was checked for various field positions. The Point Spread Function is similar to that computed with CODE V. As expected, it is best at the field edge: 7  $\mu\text{m}$  or 1/2 pixel, and more defocused on the axis.

#### 3-2-2- Direct Sun image

The image of the ideal Sun through the nominal path is not perfect, even with the best possible sampling and radial average (fig. 4). The centre is noisy, because there are few pixels to average. At the Sun edge, this noise falls to +/- 7 %. The edge is at 12.5 mm, that is 16 arcmin, but is not steep: the slope spreads over 10 arcsec, just like that of the real Sun. This shows the limits of the model sampling, rather than the imaging quality (Ch. 3-2-1).

#### 3-2-3- critical objects

Seen objects are identified by rays traced from the detector, and illuminated objects by tracing rays from various point sources (Ch. 2-5). There are many significant paths, since the filters both reflect and transmit. The number of ray impacts indicates the viewing factor.

As expected, all optical surfaces are illuminated and seen, including the detector: this will cause ghost images. The aperture stop and the secondary mirror's mount are critical. The primary mirror's back and the shutter's edge are less critical. The baffle body, near the primary, is seen and illuminated by autocollimation on the filter. The filter wheel stops are much oversized, and therefore not critical. The secondary struts are illuminated, but seen in a very small solid angle. Design improvements are discussed in (Ch. 4-3).

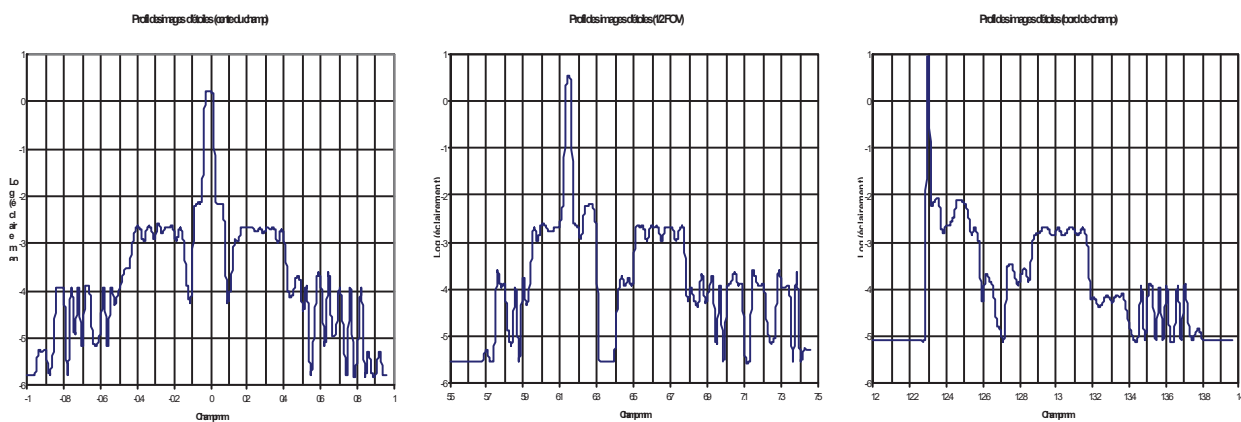
### 3-3- GHOST IMAGES

#### 3-3-1- Point source ghosts

Ray traces were done for point sources at various field angles, with 8 order splits. Ghosts basically are defocused images of the source, that is rings of increasing diameter with a central obscuration (fig. 3). The first 3 ghosts spread over 1.5 mm or 2 arcmin: this means that Sun areas at 2 arcmin from the edge can significantly contribute to stray light at the edge.

On axis, the main image is defocused, but well apart from the ghost rings. In the field, the rings remain the same but are more and more decentred, because the instrument is not telecentric. At half field, they overlap the image. At full field, all rings are tangent, slightly beyond the well-focused image.

This is not critical for aiming at stars: the first ring is 100 times darker than the star (assuming it is on a single pixel) and can easily be thresholded. However this is bad news for a broad source: stray light will spread well beyond the Sun edge, and there is no "stray image" constant in the field. The ghost signal for a broad source cannot be a simple convolution. It must be computed field by field.



A/ on axis : image and rings are separated  
 B/ 1/2 field : rings overlap the image  
 C/ Full field: rings are beyond the image

**Fig. 3 : Point source ghost images**

#### 3-3-2- ghost Paths

The main ghost paths are listed in (table 1). The filters reflect 20%, the detector is coated, and the back faces of filters are uncoated. Since extreme accuracy is needed at the Sun edge, even small contributors are significant.

Path	N°	Split level	% of total flux	% of ghosts
Nominal image	0	0	93.2	NA
Reflection Detector / Filter	R1	2	4.56	67
Reflection Detector / back of filter	R2	2	1.06	15.5
Reflection Filter / back of filter	R3	2	0.83	12.2
Reflection Detector / Filter x2	R4	4	0.2	2.87
Reflection Filter / M2	R5	1	0.05	0,77
Réfl Det / back of filter / Det / Filter	R6	4	0,05	0.67
Refl Det / Filter / Det / back of filter	R7	4	0.04	0.58
Total		1,2 & 4	6.8	100

**Table 1: Main paths in ghost images**

Angles are small and there are virtually no geometrical losses, so that paths are proportional to the combined reflectivities. Their total makes for 7% of the nominal signal. This does not prevent observing the Sun, but is well above the required radiometric accuracy. As expected, the main path is R1, but R2 and R3 are also noticeable. Together, the 1<sup>st</sup> order ghosts make for 95% of the ghost signal. Higher orders must also be estimated. R5 is an autocollimation between the filter and the secondary. It is well defocused and spread all over the detector.

### 3-3-3- Broad source ghosts

In this model, the detector is coated, the filters reflect 20% and their back faces are uncoated. The filters are in forward position. 1 million rays, order 6 splits and 3 arcsec. sampling are used. The image signal is averaged radially and normalised (fig. 4). The direct image is the same as in (Ch. 3-2-3). The ghost signal is about 7% of the direct signal, up to the edge of the Sun. It is flat with a +/- 7% noise. Then stray light falls over 1 mm, with a regular slope and no steps. Beyond this point, only high order ghosts remain. They fall over 0.25 mm with a gentler slope. Stray light does not start falling before the Sun edge, because at that point all ghosts are beyond the nominal image (Cf. Ch. 3-3-1 and 3-3-4-2).

PICARD SUN IMAGE AND GHOST  
Filter R=20% T=15% no ARC, forward position

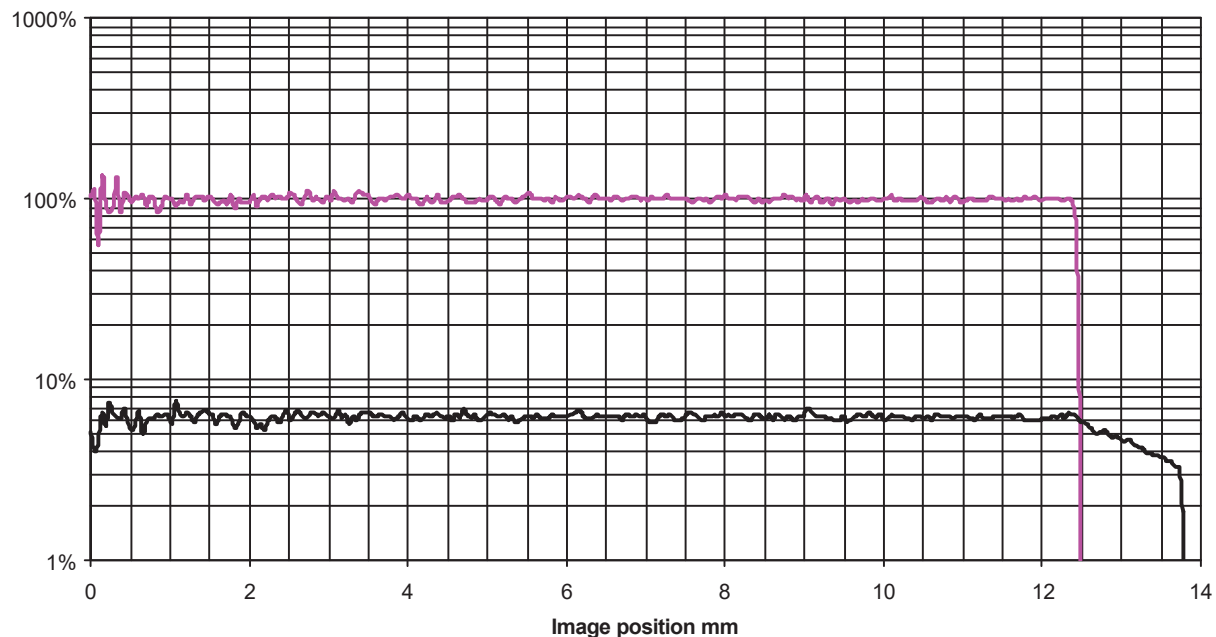


Fig. 4: Sun image and ghosts

### 3-3-4- Sensitivity to parameters

The ghost signal is proportional to the reflectivity of optical components. Several cases were modelled, but scaling just the first order (paths R1, R2 and R3) gives an order of magnitude. However, some parameters change the shape of the ghosts, and must be carefully studied.

#### 3-3-4-1: Filters reflectivity

Shifting the filters reflectivity from 20 to 30% just increases the ghost signal by 50% (fig.5) in the sun image and main slope, where 1st order ghosts (paths R1 and R3) are predominant. But it more than doubles stray light beyond 13.5 mm, where the difference is cumulated on multiple reflections. It is essential to measure both filter faces' reflectivity.

### 3-3-4-2- Filters position

The position of the filters does not change the ghosts' total energy, but they are more or less defocused. Theoretically, we may approximate the first ghost edge by the convolution of the Sun edge with the point source 1<sup>st</sup> ghost cross-section at this point, which is decentred by  $y'$ .  $D$  being the optical distance from detector to filter,  $\alpha$  the half aperture angle and  $y$  the Sun edge position,

$$\text{Defocus} = 2D \quad (3)$$

$$\text{Ring width } 2R = 2D \tan \alpha \quad (4)$$

$$\text{Ring decenter } y' = y + R \quad (5)$$

The convolution of a  $2R$  broad gate function, decentred of  $y+R$ , with a step function at  $y$  gives a linear fallout between  $y$  and  $y+2R$ .

$$\text{Ghost slope} = 1/2R = 1/(2D \tan \alpha) \quad (6)$$

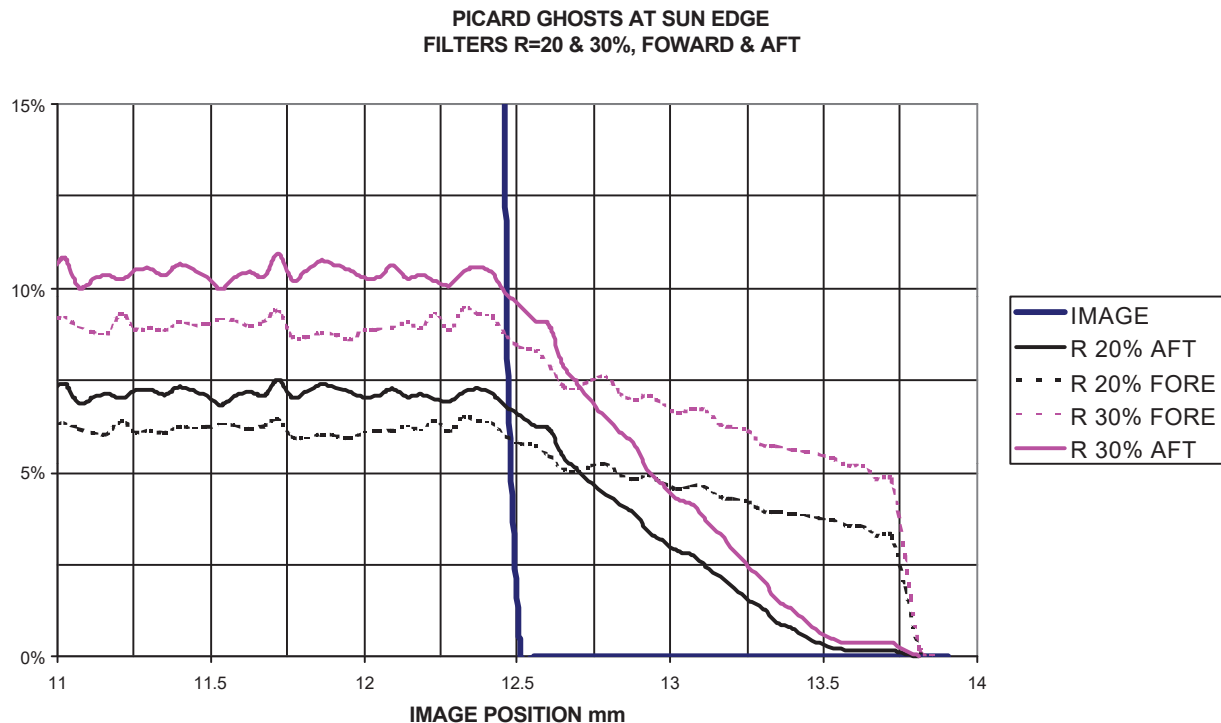
$D$  is not the actual distance, since part of the path is in the glass plate.  $Z_f$  being the position of the front face (not the filter coating),  $e$  the single plate thickness and  $n$  its optical index,

$$D = Z_{\text{det}} - Z_f - e.n/2 \quad (7)$$

The model's results are given in (fig. 5). As expected, the ghost for the aft position is less defocused and the slope is steeper. For the forward position, the slope is cut by the detector edge, and must be extrapolated. Slopes are given in (table 2). They fit well the theory, considering that the later represents only the main ghost path R1.

Filter position	D mm	Theory slope mm	Model slope mm	dSlope/ dD
Forward	12.42	3.1	2.9	0.077
Aft	37.42	1.03	1.1	0.088

**Table 2: Ghost slope versus defocus**



The ghost level in the Sun image is 6% in the forward position against 7% in the aft position, because the flux is more spread beyond the Sun, with the same total energy. It may be better to use the forward wheel to measure the Sun edge, because local stray light varies more slowly.

### 3-3-4-3- Detector coating

As expected, shifting the detector's reflectivity from 28 to 64% virtually doubles the stray light ratio. But we may also assume that this coating absorbs. This was not modelled, but approximated by scaling paths R1 and R2 (table 3). Even with a 5% reflecting detector, ghost signal is at least 1.3%. It cannot be neglected in the Sun edge measurement. It is essential to measure the detector's UV reflectivity.

R detector	Ghost scaling factor	Ghosts / Signal R Filters = 20%	Ghosts / Signal R Filters=30%
28%	1	7.3%	10.3%
15%	0.536	3.9%	5.8%
10%	0.357	2.6%	3.9%
5%	0.179	1.3%	1.9%

**Table 3: Ghost signal versus detector's reflectivity**

### 3-3-4-4- Filter's antireflective coating

If the filter's back face is coated, its contribution to the ghosts should be negligible. But if it is uncoated, a 4.3% reflectivity is not negligible compared with the filter's 20%.

As expected (fig. 6) the ghost level is increased by 1/4 without the coating, in the Sun image and the main slope. Beyond 13.5 mm there is virtually no effect, because multiple reflections on this coating are negligible. Also, the back face is closer to the detector than the filter, and its ghosts are more focused. The effect of the filter's front face is always negligible, since these ghosts paths must cross the filter twice. Thus the antireflection coating seems of little interest. However the effect of interference between the filter and the back face should be checked before making a choice.

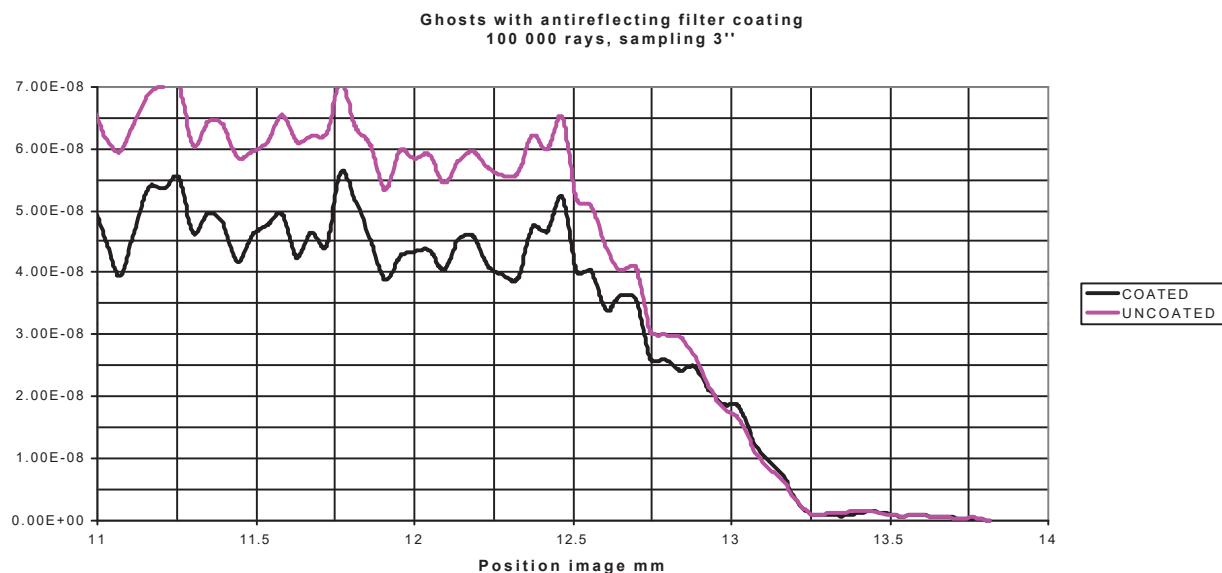


**Fig. 6: Ghosts versus Filter's back coating**

### 3-3-4-5- Filter misalignments

The instrument is very sensitive to misalignments. The detector can be finely adjusted on the telescope, but the filters may be tilted in several ways: wedged plates, tilt between the filters, filters - wheel tilt, wheel - axis tilt and bearing - instrument tilt. These are constant terms, which can be measured and compensated. But there are variable factors: thermo-mechanical instabilities and bearing clearance. Based on POLDER experience, the later might cause a random misalignment of 3 to 10 arcmin. The effects on a point source are a refraction shift of the direct image, and another shift of the ghost images, depending on their split order and on the filter - detector distance (fig. 7).

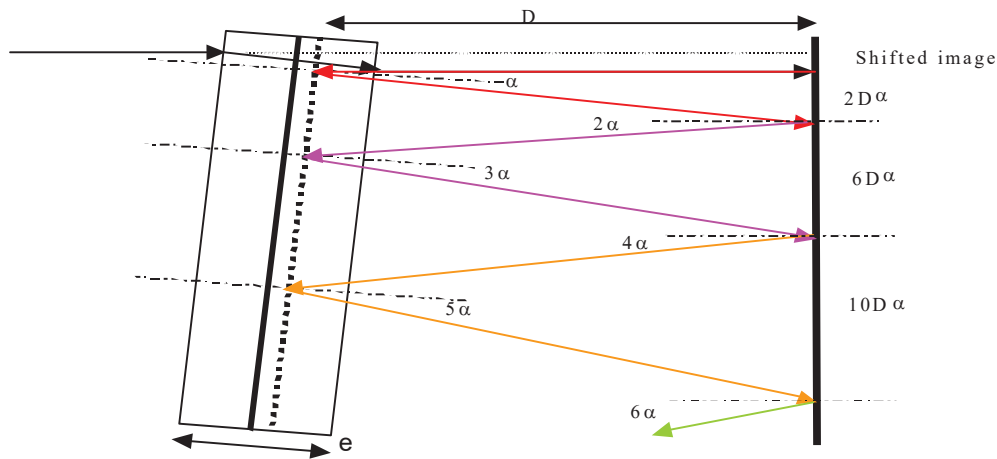


**Fig. 7: Shifts versus filter tilt**

With the notations of Ch. 3-3-4-2 and a tilt  $\alpha$  :

$$\text{Image shift: } dy_0 = e.\alpha.(n-1)/n \quad (8)$$

$$i^{\text{th}} \text{ ghost shift : } dy_i = dy_0 + (4i-2).D.\alpha \quad (9)$$

On a symmetrical broad source, the average effect is the same : non-telecentricity causes a local deviation  $\beta$  on the chief ray, equivalent to a  $(\alpha+\beta)$  tilt. Local shifts are proportional to local tilts and  $\langle\beta\rangle = 0$ . As first order ghosts are predominant, we may expect a shift of  $dy_0$  on the Sun image, and an extra shift of about  $2 D \alpha$  on the ghost image. The slope shall also be different at each Sun edge, due to a varying defocus of the ghost (cf. Ch. 3-3-4-2).  $L$  being the filter's useful diameter,

$$\Delta\text{Slope} = L.tg \alpha . d\text{Slope} / dD \quad (10)$$

The Sun image and ghosts pattern is no longer symmetrical, and radial average cannot be used. 2 million rays and a 7 arcsec. sampling gives a reasonably noisy result. The model's results are given in (fig. 8) : the filter is tilted of 20 arcmin and in forward position. The direct image shift is compensated. The untilted ghost is compared with both slopes of the tilted ghost. After compensating the ghost decenter, it also shows the slopes difference. ASAP also gives spread statistics and the weight center for each path.

GHOSTS WITH 20' TILTED FILTER  
Image shift compensated, 2 000 000 rays, pixel 7"

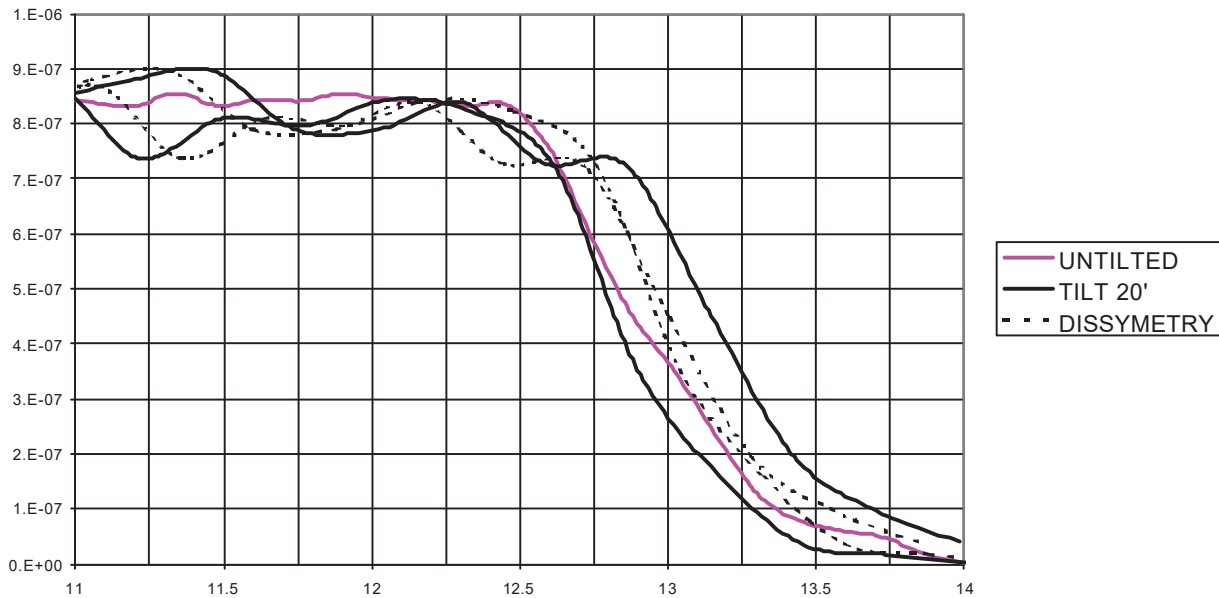


Fig. 8 : Ghost slopes versus filter tilt

As expected, the direct image is shifted of 0.016 mm. The ghost image has an extra 0.144 mm decenter, as predicted for the 1<sup>st</sup> order ghost. The ghost slopes seem slightly different, but this is hard say with a 7 μm sampling and a 14 μm expected difference. 10 arcmin tilts and other filter positions were also modelled. The image and ghost shifts have the expected order of magnitude, but the profiles are much noisy. Smaller tilts were extrapolated from theory: a 3 arcmin tilt shifts the ghost image by 1.7 pixel.

The non-symmetric pattern makes accurate modelling difficult. Predictions also require that all tilt factors are accurately known or reduced, with the required accuracy. The bearing clearance is particularly critical. As for the varying slopes, their effect is small, since at the Sun edge the ghost signal just starts falling.

### 3-4- SCATTER FROM OPTICS

Even good mirrors or filters have a micro roughness that scatters around the specular, thus enlarging the point spread function. This scatter varies in  $1/\lambda^2$ , and is more critical in the UV. Moreover it is far from isotropic: the BRDF increases rapidly close to the specular.

#### 3-4-1- General theory

According to theory [Mer00] the BRDF is proportional to the bi- dimensionnal roughness spectrum  $S(f)$ , to the reflectivity and to a polarisation factor :

$$BRDF(\theta, \lambda) = 1/\lambda^2 R \Phi S(f) \quad \text{with } f = \sin(\theta) / \lambda. \quad (11)$$

Predicting the BRDF requires knowing the roughness spectrum for the desired wavelength and angle range. This is not measured at this stage of the study. We shall use the simplest but convenient "ABC" or "Harvey-Schack" model [Har87], which just requires knowing the r.m.s. roughness  $\sigma$  and the slope  $m$ . The BRDF is a function of  $|\beta - \beta_0|$ , which is the distance to specular projected on the surface plane.

$$BRDF(\beta, \lambda) = B_0 [1 + (\beta - \beta_0) / \beta_p]^m \quad \text{with } \beta = \sin(\theta) \text{ and } \beta_0 = \sin(\text{specular}) \quad (12)$$

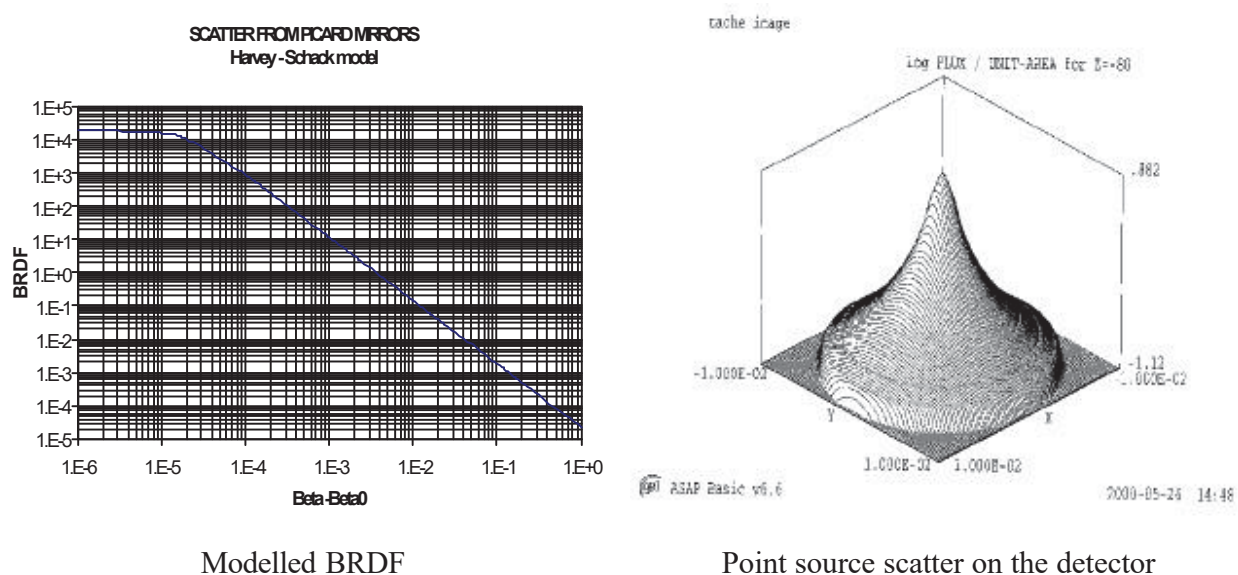
$$TIS = 1/2 \text{ spherical scatter} / R = 2\pi B_0 \beta_p^{-m} [(1 + \beta_p)^{(m+2)/2} - \beta_p^m] / R(m+2) \quad (13)$$

$$\text{TIS} = (2\pi \Delta n \sigma / \lambda)^2 \quad (14)$$

The roughness spectrum and the BRDF are assumed to be linear up to a shoulder point  $\beta_p$ . They are independent from the incidence angle and can be scaled to other wavelengths. Though wrong for high wavelengths, angles and polarisations, this model fits most measurements on smooth surfaces in the visible. Several SiC mirrors have been measured with the CNES's facility.

### 3-4-2- Near specular UV scatter

Very few measured data are available in the UV below  $0.5^\circ$  from specular. A SiC-CVD mirror was measured by the GODDARD for SOHO's SUMMER coronagraph [Lem98]. The slope is constant at -1.9, up to 2 arcsec from specular. The rms roughness is 1 nm, like PICARD's specification. Scatter at very small angles is due to low frequencies :  $0.1$  to  $10 \text{ mm}^{-1}$ . These are flatness defaults rather than micro roughness. However, measurements by REOSC on SiC-CVD mirrors show a continuous spectrum in the  $1\mu\text{m}$  to  $0.6 \text{ mm}$  range. Therefore we can assume that the BRDF regularly increases, more or less with the same slope, up to the diffraction limit.



Modelled BRDF

Point source scatter on the detector

**Fig. 9 : Mirrors scatter model**

For this study, we adopted the following "Harvey - Schack" model (fig. 9):

- **Slope:** -1.9, based on SOHO's measurement. In the visible, typical slopes are about -1.7.
- **Shoulder:**  $\beta_p = 2.10^{-5}$ . This is the sampling limit of our model.
- **Amplitude :** With specified  $\sigma = 1 \text{ nm}$  rms,  $\lambda = 230 \text{ nm}$  and  $R = 32\%$ , the hemispherical scatter is 0.1 %. This gives  $B_0 = 1.95 \cdot 10^4$ .

For the filters, there are no data on the coating' scatter, but we may assume a similar behaviour [Deum96]. The typical slope would be about -2.7, based on various visible measurements on glasses and filters. The level depends on the number of layers and on their features. A transmitting glass interface scatters 8 times less than a mirror with the same roughness, but the filter has many interfaces. As a starting point, we assumed a 0.1% hemispherical scatter, like for the mirrors, with a -2.7 slope giving  $B_0 = 10^{12}$ . The detector's scatter should be negligible.

### 3-4-3- MODELLING SCATTER

These scatter models were applied to optical surfaces, and a lambertian black model to the baffles. In ASAP, scatter is modelled by generating several rays for each impact on a surface. They are forced towards desired areas (detector or intermediate image) and weighted by the BRDF and the target solid angle [BRO99]. However, combining scatter with multiple splits rapidly increases computing time. A first run, with few rays but high order splits and scatter, proved that only the first scatter, generated or transmitted by the direct path and the first order ghosts, was significant. The

final run was performed with 200 000 rays, 10 arcsec sampling and radial average. The result looks somewhat noisy, but gives an order of magnitude.

### 3-4-4- RESULTS

As can be seen (table 4), the scattered signal is about 1.2% of the nominal signal. It is due mainly to direct scatter from the mirrors (S1, S2) and to a lesser degree from the filter (S3). This level is not surprising, as both mirrors scatter 0,1% of the signal while reflecting 32% of it. This scatter is very directive, and a significant part of it is collected in the detector's solid angle.

Path	N°	Split/scat order	% of total flux	% of scatter
Nominal image	0	0	98.69	NA
M1 scatter, direct	S1	1	0.45	37
M2 scatter, direct	S2	1	0.56	46.5
Filter scatter, direct	S3	1	0.2	16.2
Aperture top, direct	S4	1	$6.6 \cdot 10^{-5}$	0.01
Reflection / filter + M1 scatter	S5	2	0.02	1.64
Reflection / filter + M2 scatter	S6	2	0.066	5.4
M2 scatter + reflection / filter & M2	S7	2	0.025	2
Filter / M2 reflection + filter scatter	S8	2	0.01	0.82
Reflection /Det + Filter scatter	S9	2	$7 \cdot 10^{-8}$	$6 \cdot 10^{-6}$
Total scatter		1 & 2	1.22	100

**Table 4 : Main scatter paths**

Higher order split-and-scatter adds smaller contributions. Curiously, filter scatter combined with a reflection on the detector (S9) appears negligible. This might be due to geometrical factors, as the filter scatters over a wide angle towards the detector. As for the baffles, only the aperture and filter stops contribution could be identified (S4). It is  $10^{-4}$  times less than the mirrors'. These objects are far less critical than the optical components. This might make their design easier (Ch. 4).

As expected, scatter from the mirrors and filters is rather flat over the image (fig. 10), but falls near the Sun edge. This is because scatter from smooth surfaces is far from lambertian, and falls when getting away from the source.

Unlike the ghosts, scatter from the mirrors starts falling before the Sun edge, possibly because they are far from the image, and their scatter is not subject no telecentricity considerations (Ch. 3-3-1). Scatter from the stops is rather flat, but falls near the centre. This is due either to the central obscuration, or to the small number of rays sampling th central area for this path.

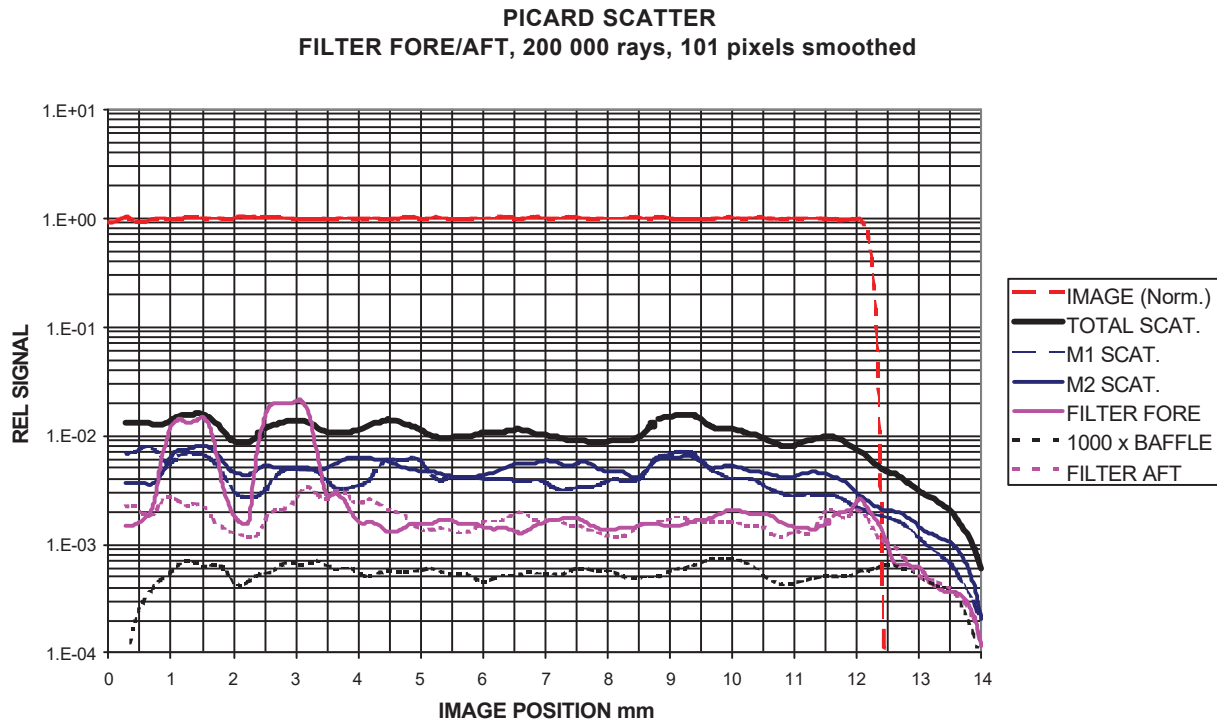


**Fig. 10 : Broad source scatter (1<sup>st</sup> order)**

The filter's scatter is quite the same for both positions, except for unexpected high levels between 1 and 3.5 mm in the forward position. This comes from isolated peaks, likely computing artefacts: changing the ray sampling moves them without suppressing them, and they do not appear for the aft filter position or for other components. No peculiar focused scattered path was identified which could explain this.

### 3-5- MODEL ACCURACY

As these ghosts cannot be suppressed, they must be predicted very accurately. Sampling with high resolution requires tracing many rays, so that enough of them can reach the studied pixels. Large areas of the Sun contribute to stray light at its edge, and must be taken as sources. With a 2 million initial rays, 6<sup>th</sup> order splits, 1<sup>st</sup> order scatter and an 3 arcsec. resolution, we reach the limits of ASAP 6.6 for this case.

#### 3-5-1- Geometrical resolution

Geometrical resolution is limited by the number of rays rather than pixel sampling (Ch. 3-3-1). A steep edge broad source gives an image with 10 arcsec. slopes. Variations in ghost slopes are not resolved. Thus there is no point in apodizing the Sun at this stage. Anyway, stray light varies more slowly, and its magnitude and behaviour were estimated. Resolution could be improved by reducing the analysis area and restricting ray generation to the locally influential Sun area (Ch. 3-3-1). But radial average would be impossible, and energy conservation should be checked for each path.

#### 3-5-2- Radiometric accuracy

Both nominal and ghost signals show variations in the Sun image, where they should be flat. This can be interpreted as sampling noise. Near the Sun edge, it is +/- 7% rms. With the same number of rays, the relative noise in the ghost image should be the same, that is +/- 0.3% of the useful signal. Besides the noise, the modelled ghost signal is very sensitive to ray sampling and to the number of splits taken into account (fig. 11). The 3<sup>rd</sup> ghost is necessary for a good estimation. As for scatter, the noise is far worse, because we sample a highly variable BRDF with few rays.



**Fig. 11 : Ghost slope versus modelling parameters**

The scattered flux can be estimated at +/-10%, but its local level would be known at +/-30 or 50% at best, that is +/-0.5% of the useful signal. Fitting a function makes things smoother, but not surer. Accurate measured data are much needed for this model (Ch. 3-5-3).

### 3-5-3- The real instrument

This model was based on preliminary data and assumptions, which were not easy to get. To be used by the real instrument, this model shall be refined, with accurate measurements on components or samples. Measurement accuracy, but also stability over the whole life, shall be very good. The important features are:

- **Optical components reflectivity** : It shall be measured in each spectral band, for each optical surface. Its uniformity over the component shall be checked. The transmission of filters is usually measured by the manufacturer. The effect of interference between the two filters shall be checked. Reflectivity shall either remain stable or be checked in flight. **NB**: In flight calibration only gives the combined evolution of transmittances and detector responsivity.
- **Roughness / scatter** : Scatter from the filter shall be measured in both half-spaces. The mirror's roughness and the BRDF shall be measured on samples, as close as possible from specular. Scatter from contamination can be predicted or measured on samples. The model shall then be updated. **NB** : If scatter cannot be measured close to the specular, it can reasonably be extrapolated linearly from scatter at higher angles.
- **Misalignments and stability** : Manufacturing and integrating may cause static misalignments. They can be measured, and their effect on ghosts either measured on the instrument or modelled. Launch and thermo-mechanical shifts cannot be measured, and shall be minimised.

The wheel bearing's clearing is especially critical, as the instantaneous axis moves randomly. Its range shall be reduced to a fraction of arcmin, to allow the desired instrument accuracy.

## 4- BAFFLES AND STRUCTURES

Some objects were identified as both illuminated by the Sun and seen from the detector, thus critical. Direct scattered paths can be suppressed or reduced, by an appropriate geometry rather than by sophisticated technologies.

#### 4-1- APERTURE STOP

It is located just before the primary mirror and scatters all over the field of view. This scatter is small compared to ghosts and mirror scatter (Ch. 3-4-4), and is more uniform and predictable. It is reduced by shadowing most of the stop with the baffle's first vane. The aperture stop could be have a super-black coating, or be very smooth with a slightly conical shape (fig. 12), so as to reflect the Sun towards the forward part of the baffle, instead of the secondary mirror and its struts. This area is not seen directly through the mirrors. Its back scatter would not be directly detected.

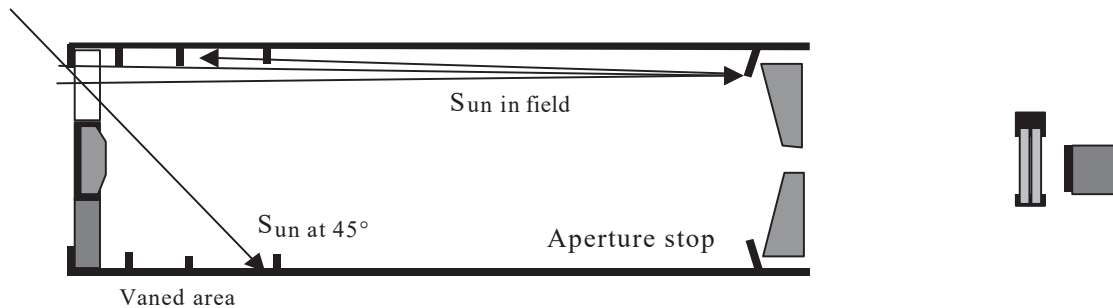


Fig. 12 : Aperture stop and vanned baffle

#### 4-2- MAIN BAFFLE

Its rear part is seen from the detector through the oversized secondary mirror, but not illuminated thanks to the entrance vane. When aiming at the Sun, it is not critical. However, when the instrument aims at stars with the Sun at  $45^\circ$  from axis, the forward part is be directly illuminated. Its scatter re-scattered in the field, mostly by the primary mirror. The specification is a  $10^{-9}$  attenuation.

This section must therefore have a vane structure, to hide it to the primary mirror (fig. 12). It cannot be hidden to the secondary mirror, but would illuminate it at high angles, so that its rescatter in the field should be very low (Ch. 3-4-2). The ideal solution is a longer baffle shadowing the secondary mirror, its struts and the main baffle. But this would increase the instrument's size and weight.

#### 4-3- SECONDARY MIRROR STRUTS

The struts are critical, as they are both directly illuminated and well in the field of view. The 4 struts are Carbon blades, parallel to the optical axis, with a glossy aspect. As the Sun is not a point source, they are illuminated at a grazing angles, and reflect into the field of view. Moreover, one of the struts carries a thermal drain which must be shadowed.

A first solution would be to tilt the blades, so as to hide the illuminated side to the primary mirror. But this would not shadow the drain, and would not work with the Sun at  $45^\circ$ . Another solution would be a "T" cross section on the inner side (fig. 13) with thin edges and a bevel turned outside. This would hide the struts to the primary mirror, whatever the Sun angle, and shadow the drain for moderate angles. For larger angles, stars observation shall wait for the drain to be in the incidence plane. The back face of the "T" would also be illuminated by a reflection on the filter. If this path is too high, a super black coating could be considered.

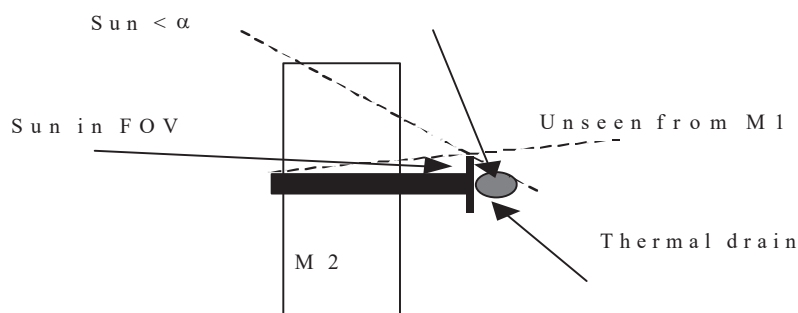


Fig. 13 : Struts with "T" cross section

Both solutions would increase the obscuration ratio and the diffraction spot. As the viewing angle of the present struts is small, a trade-off should be studied between stray light and diffraction with dedicated ray traces.

## 5- CONCLUSION

This study was based on preliminary data and design. It demonstrates that ghost images between the detector and the filters, and scatter from the optical components, cause several percent stray light with a non uniform profile. This is not critical for point sources, but on a broad source it will bias the Sun edge, which must be measured at  $10^{-3}$  arcsec. As this stray light cannot be suppressed nor much reduced with the present design, it shall be predicted very accurately, then included in the image processing.

Our model of ghost images had +/- 0.3% absolute accuracy with 3 arcsec. sampling. This could be improved with more locally aimed ray tracing and sampling, and measured data on the components. The centring of ghost images is also very sensitive to filters misalignments. Constant tilts could be measured and taken into account, but variable ones shall be minimised. Scatter is by nature harder to predict accurately. It would require BRDF measurements on samples and contamination wafers. Finally, full scale test on the instrument could confirm and refine the predictions.

## REFERENCES

- [Spy75] : **Scatter from particulate contaminated mirrors**  
P.R. Spyak, Optical engineering n°31/8, 1975
- [Har87] : **Surface scatter phenomena : a linear, shift-invariant process.**  
J.E. Harvey, SPIE 1165, 1989.
- [Deum96] : **Multiscale roughness in optical multilayers : atomic force microscopy and light scattering**  
C. Deumier & al., Applied optics vol. 35 N°28, 1/10/96
- [Dam98] : **Picard: Simultaneous measurements of the solar diameter, differential rotation, solar constant and their variations**  
L. Damé & al. 32 Th. COSPAR, Nagoya, Jul. 1998 (Adv. in Space Research 24, 1999)
- [Lem98] : **La lumière parasite dans le domaine UV pour SOHO :le spectromètre UV SUMER**  
P. Lemaire (IAS) : Stray light workshop, Toulouse, 8/12/98
- [BRO99] : **BRO : ASAP 6.6.1 reference manual**
- [Koz99] : **Comparative study of the roughness of optical surfaces and thin films using atomic force microscopy, X ray scattering and light scattering methods.**  
I.V. Kozhevnikov & al, SPIE 3739, may 99
- [Dam00] : **Picard microsatellite program**  
L. Damé, M. Meissonnier, B. Tatry, 5<sup>th</sup> International Symposium Small on Satellites and Services, La Baule, June 2000
- [Act00] : **ACTON Research Corporation, products**  
<http://www.acton-research.com/pdfindex.html>
- [Mer00] : **Intercomparaison des mesures de diffusion et de rugosité.**  
R. Mercier, IOTA, rapport final du contrat 961/CNES/94/1358/00